Ion-ion interaction and equation of state of a dense plasma: Application to beryllium

F. Perrot
Centre d'Etudes de Limeil-Valenton, 94195 Villeneuve St-Georges CEDEX, France
(Received 27 January 1992; revised manuscript received 16 September 1992)

A recent model treating the structure of "simple plasmas" as that of high-temperature liquid metals is used here to calculate the equation of state of dense beryllium plasmas, for values of compression between 0.2 and 6, and temperatures up to 100 eV. This model gets rid of the standard simplified descriptions of ionic distributions (isolated ion sphere, uniform positive background, etc.); it applies when the electronic structure justifies the use of a binary pair interaction. This interaction is calculated, for every density and temperature, using the self-consistent electronic charge density obtained in a density-functional-theory calculation. The statistical mechanics of the ion fluid is treated via a modified hypernetted-chain integral equation. The various contributions to the equation of state are presented and discussed, and comparisons with other theories are made.

PACS number(s): 52.25.Jm, 05.70.Ce, 52.25.Kn, 61.20.Ne

I. INTRODUCTION

The general method for constructing an equation of state (EOS) in a wide domain of densities and temperatures consists in adding three contributions: (i) a term representing the zero-temperature isotherm, (ii) a thermal electronic component, and (iii) a thermal ionic part. Though more or less sophisticated models can be chosen for calculating these various pieces, they are in general derived independently and without intrinsic coherence [1]. For instance, the zero-temperature part is calculated using solid-state band-structure theory, and the thermal electronic part is obtained in a statistical Thomas-Fermi model (possibly with corrections). Then, a thermal ionic free energy interpolating between those of the hard-sphere (HS) fluid and the Coulomb one-component plasma (OCP) is added. The problem to solve is so difficult that this kind of approach is often the only tractable one and may be of great practical interest if fitted parameters are included.

The INFERNO model of Liberman [2] improves the internal coherence of these calculations, at least for metallic systems, by applying the same theory to the electrons, on the 0-K isotherm and for any finite temperature. But the description of the average environment around an atomic sphere leads to difficulties in the definition of thermodynamic functions. The notion of ion-ion interaction is not included in this model, which has become a reference in the field of EOS calculations.

An alternative approach to the treatment of the interaction between an atom and its environment is possible, at least in a large part of the density-temperature domain of interest, in cases where the electronic structure of the material is "simple," that is, when the conduction electrons are all free-electron-like and do not hybridize with localized states. In this work, we use this approach for Be plasmas.

The treatment of the effective ionic interactions is at the center of this study. We have applied a model originally proposed to describe the solid phase of simple metals [3], also applied to the liquid phase of these metals [4], and extended to the domain of dense plasmas [5] where the ionization changes with density and temperature. The model deals with constructing the effective ion-ion interaction, for any set of density and temperature parameters, starting from the self-consistent electron charge density previously calculated using density-functional theory for a single neutral pseudoatom.

The model is applicable to plasmas with densities in the metallic range, temperatures higher than a few eV, and intermediate ion-ion coupling (for strong coupling, the common isolated ion-sphere model is expected to work well, and for weak coupling the ionic nonideal contribution is not very important).

The paper is organized as follows. In Sec. II we recall the most important features of the model, presented and discussed at length in Ref. [5]. In Sec. II E we shall describe a modification of the model that we found relevant to include: we now solve a modified hypernetted-chain (MHNC) equation, instead of a HNC equation, for the ionic structure. Including bridge terms is known to be important in regimes of strong ionic coupling, in particular for the liquid metal close to freezing, where the model will be shown to give reasonable results. In Sec. II F we derive specific formulas for the internal energy E and the pressure P from the Helmholtz free energy F which is the basic quantity of the theory. This derivation was absent in Ref. [5] where results for F only were given. E and P are to a large extent calculable explicitly, as a consequence of the variational properties of the model. But a part of the free energy, the variations of which being made as weak as possible, must be differentiated numerically. This is the price to pay for the treatment of the temperature-dependent effective interaction. Section III is devoted to estimating the accuracy of the method through a comparison between its results on the 0-K isotherm and those of other theories and measurements. A test case for liquid Be at freezing is also presented. The dense beryllium plasma phase is the subject of the last section, for compressions going from 0.2 to 6, and tem-

peratures between 2.5 and 100 eV. The numerical results are discussed; the thermal electronic component is compared with other estimates. Values of the total thermodynamic functions are tabulated and their changes with respect to a simple Be EOS are shown. Finally, some remarks on the validity of the model are given as a conclusion.

II. THE MODEL

Although its limitations for dense systems are well known, the approximation of binary ion-ion interactions (BIIA) remains the only one that can be practically used, when justified, for constructing an EOS of wide use in hydrodynamic applications. Its numerical implementation is already rather complex, as will be seen in this paper. Let us start with a brief description of the physical model.

A. Physical content

The model has been presented in great detail in Ref. [5]. Here we only recall the main assumptions and results of the derivation. The BIIA appears naturally in the study of simple metals, when second-order perturbation theory is applied to the electron-ion interaction represented by a weak pseudopotential. The present model deals with the same class of systems, but treats the electron-ion interaction to all orders using density-functional theory (DFT) [6]. The BIIA implies that the total electron density of the system is given as a superposition of rigid one-site densities.

$$n(r)=\sum_i \Delta n(\mathbf{r}-\mathbf{R}_i)=\sum_i \Delta n_i \tag{1}$$

centered on all the sites $\mathbf{R}_i$. Such a superposition approximation is kept in the present model, where the individual density is written

$$\Delta n(r)=\Delta n^*(r)+m(r) . \tag{2}$$

Δn^* and m are chosen in order to fulfill the following requirements. (i) Δn^* is made of a bound contribution n_b and a delocalized contribution Δn_f^*. The total charge carried by Δn_f^* is zero.

$$\int_\infty \Delta n_f^* d\mathbf{r}=0 . \tag{3}$$

(ii) m is such that the overlap $\sum_i m(\mathbf{r}-\mathbf{R}_i)=\sum_i m_i$ is not very different from the uniform average density $\bar{n}$ in the system.

The distribution Δn^* is the electron charge density of the so-called "neutral pseudoatom" (NPA). A *single* NPA results from the external potential

$$\frac{1}{r}*(-Z\delta+\nu-\bar{n}) , \tag{4a}$$

which, when screened by $\bar{n}+\Delta n^*$, becomes

$$V^*=\frac{1}{r}*(-Z\delta+\nu+\Delta n^*) . \tag{4b}$$

δ is a Dirac distribution and the symbol * is used for the convolution product

$$f*g=\int f(\mathbf{r}')g(\mathbf{r}-\mathbf{r}')d\mathbf{r}' .$$

Z is the nucleus charge and $\nu(r)$ a screening charge density which totally screens the ion. It carries the net charge Z^*,

$$Z^*=\bar{n}\Omega , \tag{5}$$

where Ω is the average atomic volume, so that

$$Z^*=Z-\int_\infty n_b(r)d\mathbf{r}=\int_\infty \nu(r)d\mathbf{r} . \tag{6}$$

The total charge neutrality implies Eq. (3). Thus the NPA Fiedel sum is zero: the NPA is a very weak scatterer. Let us rewrite Eq. (1) in the following form:

$$n(\mathbf{r})=\left[\bar{n}+\sum_i \Delta n_i^*\right]+\left[\sum_i m_i-\bar{n}\right] . \tag{7}$$

Because the pseudoatoms are weak scatterers, their density contributions are additive, so that $\bar{n}+\sum_i \Delta n_i^*$ can be considered as the density of an assembly of pseudoatoms for which the external potential is

$$V_{\text{ext}}^*=\frac{1}{r}*\left[\sum_i(-Z\delta_i+\nu_i)-\bar{n}\right] . \tag{8}$$

The remaining part of the total density in Eq. (7), $\sum_i m_i-\bar{n}$, is treated in linear response. The corresponding external potential δV_{ext} is the difference between the exact external potential of the system

$$V_{\text{ext}}=\frac{1}{r}*\left[\sum_i -Z\delta_i\right]$$

and V_{ext}^*,

$$\delta V_{\text{ext}}=V_{\text{ext}}-V_{\text{ext}}^*=\frac{1}{r}*\left[\sum_i \nu_i-\bar{n}\right] , \tag{9}$$

which is weak by construction. Thus

$$m(r)=(2\pi)^{-3}\int d\mathbf{q}\frac{\Pi_0(q)}{\epsilon(q)}\frac{4\pi}{q^2}\nu(q)e^{-i\mathbf{q}\cdot\mathbf{r}} , \tag{10}$$

where $\Pi_0(q)$ is the density response function of the uniform electron gas at density $\bar{n}$ and temperature T, and

$$\epsilon(q)=1-\left[\frac{4\pi}{q^2}+X\right]\Pi_0(q) , \tag{11}$$

with X the local-field factor consistent with the exchange-and-correlation (xc) approximation used in the NPA calculation. Here, we have adopted the local density approximation (LDA), with the numerical fit due to Iyetomi and Ichimaru [7] for the xc functional $F_{\text{xc}}(\bar{n},T)$.

The screening charge $\nu(r)$ is chosen as a sphere with uniform density of charge $\bar{n}$, so that its radius R is equal to the average atomic radius in order to satisfy Eq. (5),

$$\nu(r)=\begin{cases}\bar{n} & \text{for } r<R\\ 0 & \text{for } r\geq R .\end{cases} \tag{12}$$

The calculation of the NPA density profile Δn^* is done by solving the DFT equations, for a spherical scattering center in a uniform electron gas, using standard tech-

niques [8]. This can be done either at zero temperature (Hohenberg-Kohn-Sham equations) or at finite temperature (Mermin-Kohn-Sham equations). When Δn^* for a single NPA is obtained, it is easy to calculate the "embedding free energy" of a NPA, defined as the difference between the free energy of the electron gas containing the NPA and that of the uniform electron gas:

$$F_1 = G[\bar{n}+\Delta n^*] - G[\bar{n}] - \frac{Z}{r} \circ (\Delta n^* + \nu) + \tfrac{1}{2}(\Delta n^* + \nu) \circ \frac{1}{r}_* (\Delta n^* + \nu) \ . \quad (13)$$

The symbol $\circ$ stands for integration in whole space,

$$f \circ g = \int_\infty f(r) g(r) d\mathbf{r} \ .$$

In Eq. (13), $G[n]$ is the functional containing the kinetic noninteracting free energy plus the xc free energy F_{xc}. A detailed expression of F_1, readily calculable, is given in Appendix A.

B. Plasma electronic free energy

In this section we summarize the derivation of a formula for the plasma (or liquid metal, or solid according to temperature) free energy, in a given distribution of the ions $(\ldots \mathbf{R}_i \ldots)$. This free energy is made of (i) the G contribution, the energy of the electrons in the external potential V^*_{ext}, the electron-electron interaction for all the pseudoatoms,

$$G\left[\bar{n} + \sum_i \Delta n_i^*\right] + \left[\bar{n} + \sum_i \Delta n_i^*\right] \circ V^*_{ext} + \frac{1}{2}\left[\bar{n} + \sum_i \Delta n_i^*\right] \circ \frac{1}{r}_* \left[\bar{n} + \sum_j \Delta n_j^*\right] ; \quad (14a)$$

(ii) the second-order perturbation free energy associated with δV_{ext},

$$\delta F_e = \left[\bar{n} + \sum_i \Delta n_i^*\right] \circ \delta V_{ext} + \frac{1}{2}\left[\sum_i m_i - \bar{n}\right] \circ \delta V_{ext} \ ; \quad (14b)$$

and (iii) the nuclei interaction energy

$$\tfrac{1}{2} \sum_{i,j}{}' Z^2 / R_{ij} \ . \quad (14c)$$

The main problem in calculating this free energy comes from the G contribution, due to the overlap of densities. The advantage of the NPA is that the following expansion is a fairly good approximation:

$$G\left[\bar{n} + \sum_i \Delta n_i^*\right] = G[n] + \sum_i \{G[\bar{n} + \Delta n_i^*] - G[\bar{n}]\} + \tfrac{1}{2} \sum_{i,j}{}' G_{ij} \ , \quad (15)$$

where the third- and higher-order terms in a full cluster expansion are negligible. The validity of this truncated expansion, discussed by Dagens [3], comes from the fact that the overlapping part Δn_f^* of Δn^* has a vanishing integrated charge and is displaced by a weak scattering center. Equation (15) is not applicable if this condition is not satisfied. All the above contributions can be rearranged to give, as shown in Appendix B, the total free energy per atom in a fixed ionic configuration:

$$F_e = F_0 + F_1 + \tfrac{1}{2} \sum_j{}' \phi(R_j) + (\bar{n} - \nu) \circ V^* - \tfrac{1}{2}(\bar{n} - \nu) \circ \frac{1}{r}_* (\nu - m) \ , \quad (16a)$$

$$F_0 = Z^* g(\bar{n}, T) = Z^* [g_t(\bar{n}, T) + g_{xc}(\bar{n}, T)] \ . \quad (16b)$$

F_0 is the free energy of Z^* electrons in a uniform electron gas, with a kinetic part g_t and an xc part g_{xc}. F_1 is defined in Eq. (13), and ϕ is a binary interaction, the formal expression of which is given in Appendix B.

C. Ionization

The usual definition of the number of free electrons in a simple metal (or plasma) is given in Eq. (6) which applies if there is no ambiguity when sharing the spectrum into bound and free parts. But, for particular values of the density and temperature parameters, bound levels cross the zero-energy limit and enter the continuum (pressure ionization), or vice versa (temperature localization of effective eigenstates). In the NPA calculation, these transitions are associated with the appearance of resonances in the continuum, which reflect the existence in the plasma of a band of electronic levels weakly bound to a cluster of ions ("hopping" states) [9]. The present model, though it is unable to describe such complex situations where the BIIA may break down, can nevertheless apply when bound levels begin to interact weakly between adjacent sites. It has been shown in Ref. [5] that this effect may be accounted for by changing the definition of the bound and free densities:

$$\Delta n^* = n_b + \Delta n_f^* = f n_b + [(1-f) n_b + \Delta n_f^*] \quad (17a)$$

$$= n_b' + \Delta n_f^{*\prime} \ , \quad (17b)$$

where f is a "cutting" function

$$f = [1 + \exp(-1/\alpha)] / \{1 + \exp[(r - R)/\alpha R]\} \ , \quad (18)$$

with $\alpha = 0.05$. The charge density n_b' is now considered as "truly" rigid, and $\Delta n_f^{*\prime}$ as responding to external perturbations. The ionization is given by Eq. (6) with n_b' instead of n_b, and Δn_f^* must be replaced with $\Delta n_f^{*\prime}$ in Eq. (3), without any other change in the model.

When the overlap between bound levels on different sites becomes too strong, or when too sharp resonances do appear in the NPA continuum, the model is no longer valid; examples will be seen below in the numerical applications.

D. Ion-ion interaction

The interaction defined in Appendix B is not calculable without further approximation, because the two-body kinetic and xc term G is not known explicitly. The solution to this problem is to introduce an auxiliary pseudopotential $w(q)$ which, if used in linear response theory, repro-

duces the "exact" NPA free-electron density given by DFT calculation:

$$w(q)=\frac{\epsilon(q)}{\Pi_0(q)}\Delta n_f^{*\prime}(q) , \tag{19}$$

with the same ϵ and Π_0 as in Eq. (11). With such a definition, the ion-ion interaction is found to be [with $v(q)=4\pi/q^2$]

$$\phi(q)=(Z^*)^2v(q)+\frac{\Pi_0(q)}{\epsilon(q)}[w(q)-v(q)\nu(q)]^2 , \tag{20}$$

where the quantity in brackets plays the role of the bare ionic pseudopotential. The approximation is expected to work if

$$a(q)=-[w(q)-v(q)\nu(q)]/Z^*v(q) \tag{21}$$

is smaller than 1 for any q. More details concerning the practical aspects of the interaction calculation can be found in Ref. [5].

E. Ionic structure

The last step in the calculation of the total free energy F of the plasma is to average the electronic free energy F_e (defined for a given set of ionic positions) on the ionic coordinates [10]. This requires the knowledge of the ion pair distribution $g(r)$. Most of the plasma studies with integral equations use the hypernetted-chain equation [11–15]; this was the approach chosen in Ref. [5]. But the HNC approximation can be improved for strong-coupling regimes by taking a bridge function $B(r)$ into account in the so-called modified hypernetted-chain equations [16]. We have adopted this scheme in the formulation of Lado, Foiles, and Ashcroft [17]. These authors have derived a criterion for selecting the packing fraction η of an auxiliary hard-sphere system, the bridge function $B_{\rm HS}(r;\eta)$ of which is used in the MHNC equations. They have also given a variational expression of the ionic free energy $F_{\rm pair}$. The packing fraction is determined by

$$0=\int d\mathbf{r}\frac{\partial B_{\rm HS}(r;\eta)}{\partial\eta}[g(r)-g_{\rm HS}(r)] . \tag{22}$$

The bridge function of the HS system can be computed with the help of the accurate numerical fits given by Verlet and Weis [18], and Henderson and Grundke [19]. The free energy is

$$\beta F_{\rm pair}=\frac{3-2\eta}{(1-\eta)^2}-3+\beta F_r[h]-\beta F_r[h_{\rm HS}] +\beta F_q[h]-\beta F_q[h_{\rm HS}] , \tag{23a}$$

$$\beta F_r[h]=-\tfrac{1}{2}\bar\rho\int d\mathbf{r}[-\tfrac{1}{2}h^2(r)+g(r)c(r)] , \tag{23b}$$

$$\beta F_q[h]=-\frac{1}{2\bar\rho}(2\pi)^{-3}\int d\mathbf{q}\{\ln[1+\bar\rho h(q)]-\bar\rho h(q)\} , \tag{23c}$$

where $h(q)$ is the Fourier transform of $h(r)=g(r)-1$, $c(r)$ the direct correlation function, $\bar\rho$ the ionic density $1/\Omega$, and $\beta^{-1}=k_BT$. The definition of the interaction average

$$\langle\phi\rangle=\tfrac{1}{2}\bar\rho\int\phi(r)d\mathbf{r}=\tfrac{1}{2}\bar\rho\phi(q=0) \tag{24}$$

will be needed below. These MHNC equations, commonly used in liquid metal studies [20–24], recently applied to Coulombic plasmas with linear electronic screening [25], have been used systematically in the present work.

F. Internal energy and pressure

Next we show how the EOS functions, internal energy and pressure, may be practically obtained starting from the total free energy

$$F=F_0+F_1+F_{12}+F_{\rm id}-E_{\rm at} , \tag{25}$$

with F_0 given in Eq. (16b), F_1 in Eq. (13), and

$$F_{12}=F_{\rm pair}+(n-\nu)\circ V^*-\tfrac{1}{2}(n-\nu)\circ\frac{1}{r}*(\nu-m) . \tag{26}$$

$F_{\rm id}$ is the ionic ideal contribution and $E_{\rm at}$ is the energy of an isolated atom in its $T=0$ ground state, obtained in a separate calculation with the same xc approximation, and chosen as reference energy. Since the ionization Z^* is a function of density and temperature, we must introduce two functions:

$$\gamma_T=\frac{T}{Z^*}\left[\frac{\partial Z^*}{\partial T}\right]_\Omega , \tag{27a}$$

characterizing the variations of Z^* with temperature at constant volume, and similarly

$$\gamma_\Omega=\frac{\Omega}{Z^*}\left[\frac{\partial Z^*}{\partial\Omega}\right]_T . \tag{27b}$$

These functions may be reexpressed in terms of the derivative with respect to the input variable $\bar n$ [from which Ω is defined by Eq. (5)]:

$$\gamma_T=\frac{T}{Z^*}\left[\frac{\partial Z^*}{\partial T}\right]_{\bar n}(1-\gamma_{\bar n})^{-1} , \tag{27c}$$

$$\gamma_\Omega=-\gamma_{\bar n}(1-\gamma_{\bar n})^{-1} . \tag{27d}$$

The internal energy associated with F_0 is obviously

$$\frac{\partial}{\partial\beta}(\beta F_0)=E_0-\mu Z^*\gamma_T , \tag{28}$$

where E_0 is the "normal" energy of a constant number Z^* of electrons in an interacting uniform electron gas, to which a term due to the variations of Z^* with temperature is added; μ is the chemical potential of the electron gas

$$\mu=\frac{\partial}{\partial\bar n}[\bar n g(\bar n,T)] .$$

Similarly, the pressure is given by

$$-\left[\frac{\partial F_0}{\partial\Omega}\right]=(1-\gamma_\Omega)P_0-\gamma_\Omega F_0/\Omega . \tag{29}$$

where P_0 is the "normal" pressure (at constant Z^*) of the electron gas.

When the energy E_1 associated with F_1 is calculated, a first contribution, $\tilde{E}_1$, comes from $\partial(\beta F_1)/\partial\beta$ at constant $\bar{n}$ and Z^*. This "normal" term is given in Appendix A. An additional term comes from the change in $\bar{n}$, Z^*, and Ω. The corresponding variations in F_1, starting with Eq. (13), are

$$\delta F_1 = \delta G[\bar{n}+\Delta n^*] - \delta G[\bar{n}] + (\delta\Delta n^* + \delta\nu)\circ V^* = \mu\delta\Delta n^* - (\delta\bar{n} - \delta\nu)\circ V^* , \tag{30a}$$

which becomes, with the help of Eq. (12),

$$\delta F_1 = -\mu\delta Z^* - (\bar{n}-\nu)\circ V^* \frac{\delta\bar{n}}{\bar{n}} + \bar{n}V^*(R)4\pi R^2\delta R . \tag{30b}$$

For calculating E_1 (at constant volume), $\delta R = 0$, so that

$$\frac{\partial}{\partial\beta}(\beta F_1) = \tilde{E}_1 + \gamma_T[\mu Z^* + (\bar{n}-\nu)\circ V^*] . \tag{31}$$

In the expression of the pressure P_1, there is no "normal" contribution at $\bar{n}$, Z^*, β fixed because there is no explicit volume dependence in F_1 other than those shown in Eq. (30b). Thus P_1 is

$$-\Omega\left[\frac{\partial F_1}{\partial\Omega}\right]_T = \gamma_\Omega\mu Z^* - (1-\gamma_\Omega)(\bar{n}-\nu)\circ V^* - Z^*V^*(R) . \tag{32}$$

The last term in the free energy, F_{12} is resistant to explicit derivation because of the complex implicit T dependence of the pair interaction. As a consequence, the corresponding E_{12} and P_{12} must be computed numerically. Fortunately, F_{12} varies much more slowly with $\bar{n}$ and T than F_{pair} alone, so that the accuracy on E_{12} and P_{12} does not suffer from numerical differentiation. Gathering all the results of this section, we obtain

$$E = E_0 + E_1 + E_{12} + E_{\text{id}} - E_{\text{at}} , \tag{33a}$$

$$P = P_0 + P_1 + P_{12} + P_{\text{id}} , \tag{33b}$$

$$E_1 = \tilde{E}_1 - \gamma_T P_a\Omega , \tag{34a}$$

$$P_1 = P_a + (1-\gamma_\Omega)P_b , \tag{34b}$$

$$E_{12} = \frac{\partial}{\partial\beta}(\beta F_{12})_\Omega , \tag{35a}$$

$$P_{12} = -\frac{\partial}{\partial\Omega}(F_{12})_T , \tag{35b}$$

$$P_a\Omega = -(\bar{n}-\nu)\circ V^* , \tag{36a}$$

$$P_b\Omega = -Z^*V^*(R) . \tag{36b}$$

E_0 and P_0 are relative to Z^* electrons in a uniform electron gas. A detailed form of $\tilde{E}_1$ is given in Appendix A.

III. ZERO-TEMPERATURE ISOTHERM AND LIQUID METAL

The method described in the preceding section has been applied to beryllium. The extremely stable electronic structure of this material is favorable in the treatment of the fluid phase: there exists a wide domain of densities and temperatures where the only bound level is the 1*s* level, the continuum states coming to a large extent from the delocalization of the 2*s* level. On the contrary, the solid phase band structure, less free-electron-like than that found in alkali metals, and the low density of states at the Fermi level, make of Be a nontrivial candidate for applying the present method. In this section we report the results obtained at $T=0$ K as a test of the model. The reference electron density is $\bar{n}_0 = 0.038\,48$ a.u. corresponding to the volume $\Omega_0 = 51.9751$ a.u. and to the material density $\rho_0 = 1.9438$ g/cm^3.

A. Pair interaction energy

At zero temperature, F_{pair} reduces to

$$E_{\text{pair}} = \tfrac{1}{2}\sum_X{}' \phi(X) , \tag{37}$$

where the X are the lattice vectors. This sum can be calculated more accurately in reciprocal space. The difficulty of the calculation is that it requires the determination of the most stable lattice. We have compared a limited number of structures: fcc, bcc, and hexagonal with a variable ratio c/a. It was found that, at normal density, the hcp structure [$c/a = 2(\frac{2}{3})^{1/2} = 1.633$] is the most stable, in agreement with experiment [26] (but the measurements give a c/a ratio slightly smaller, 1.579, than the ideal value). Computations indicate that the hcp structure remains the most favorable up to compression 3 where the bcc lattice begins to be more stable. The most recent experiments indicate a transition from hcp towards a hexagonal phase with $c/a = 0.9$ at $\rho/\rho_0 = 1.17$ [26]. Such a transition has not been found in the calculations. There is no experimental result at $\rho/\rho_0 = 3$ on the 0-K isotherm, and the only possible comparison is with other theoretical estimates. It has been found, using the augmented-spherical-wave (ASW) method [27] that the hcp→bcc transition occurs for compression 1.55, a value significantly lower than that predicted by the present work.

TABLE I. Pair interaction energy E_{pair} (Ry) at $T=0$ K in Be, for various structures.

Structure	c/a	$\bar{n}/\bar{n}_0 = 1$	$\bar{n}/\bar{n}_0 = 3$	$\bar{n}/\bar{n}_0 = 0.8$
fcc		−0.021 56	0.3620	−0.031 75
bcc		−0.020 64	0.3385	−0.027 74
Hexagonal	1.4			−0.035 05
	1.5	−0.028 24	0.3427	−0.035 66
	1.6	−0.028 78	0.3387	−0.035 68
	1.7	−0.028 58	0.3418	−0.035 90
	1.8			−0.036 60
	1.9			−0.037 30

For densities lower than the normal value, calculations show that the hexagonal phase is also the most stable. But the value of c/a minimizing the energy increases very fast with decreasing density. This ratio exceeds 2 as soon as compression reaches 0.8, as if the material were developing a tendency towards a more and more planar structure. But here again, no experimental evidence is available, so that this result must be taken with care.

As an illustration, Table I shows a comparison of the energies in various structures for the three densities $\bar{n}/\bar{n}_0 = 1$, 3, and 0.8.

Owing to the particular behavior found for compressions lower than 1, and because we do not have the answer to the question of whether there is any other structure which could be more stable, we have chosen to use the pair energy of a hexagonal lattice with $c/a = 1.9$ in the zero-temperature tabulations (Table II). This choice has no important consequence since these densities are never reached in the solid phase.

B. Equation of state at 0 K

In Table II we show the various contributions to the Be EOS at $T = 0$ K, for compressions in the range 0.2–6. In this range, Z^* varies from 2.000 to 2.033. The isolated free-atom energy taken as reference is $E_{at} = -28.8921$ Ry. The results may be compared with those obtained using a band-structure method, the linearized muffin-tin orbital (LMTO) method [28]. The pressure given by this method has been integrated to get the energy E, with an integration constant chosen to give the experimental cohesive energy at compression 1 [29]. The zero-point energy (0.011 Ry at normal density) is not included. Good agreement can be noticed, on both E and P. We can also remark that the cohesive energy calculated by Moruzzi, Janak, and Williams [30], using the KKR (Korringa-Kohn-Rostoker) method, is -0.310 Ry for the fcc phase, more different from the experiment, -0.259 Ry [29], than the value found in this work, -0.281 Ry. The bulk modulus at zero pressure found here is 1.30 Mb, to be compared with 1.31 Mb computed by Moruzzi and 1.01 Mb, experimental value (both corrected for the vibration contribution).

Finally, we display in Fig. 1 the effective pseudopotential used for calculating the pair interaction, as defined in Eq. (21), for compressions 1 and 3. One can see that $a(q)$ remains smaller than 1 in magnitude. This is the condition required for the validity of the approximation.

The comparison of the results obtained here with those of other methods, and also with experimental data, indi-

TABLE II. Beryllium equation of state at $T = 0$ K. The tabulated quantities are defined in Eqs. (33a) and (33b). The LMTO data are those of Ref. [28]. Ω and $\bar{n}$ correspond through relation $Z^* = \Omega\bar{n}$, and $\Omega_1 = 52.0952$ a.u. is the LMTO equilibrium volume. Energies are in Ry and pressures in Mb. The electronic density $\bar{n}$ is in a.u.

Ω_1/Ω	E_0	$E_1 - E_{at}$	E_{12}	E	LMTO
0.200	−0.2781	0.1398	0.0853	−0.0531	
0.401	−0.1836	−0.0656	0.0862	−0.1630	
0.601	−0.0796	−0.2228	0.0666	−0.2359	
0.802	0.0251	−0.3446	0.0480	−0.2715	
1.002	0.1286	−0.4406	0.0309	−0.2811	−0.2592
1.203	0.2304	−0.5182	0.0153	−0.2725	−0.2508
1.403	0.3304	−0.5832	0.0028	−0.2500	−0.2297
1.603	0.4285	−0.6392	−0.0072	−0.2179	−0.1991
1.803	0.5250	−0.6882	−0.0152	−0.1784	−0.1603
2.003	0.6198	−0.7313	−0.0211	−0.1326	−0.1149
2.998	1.074	−0.8718	−0.0308	0.1714	0.1787
3.983	1.503	−0.9458	−0.0231	0.5339	0.5332
5.917	2.313	−0.9999	0.0245	1.337	1.347
$\bar{n}$	P_0	P_1	P_{12}	P	LMTO
0.007 70	0.0455	−0.1297	0.0129	−0.0713	
0.015 39	0.2303	−0.4094	−0.0293	−0.2085	
0.023 09	0.5331	−0.7088	−0.0969	−0.2727	
0.030 78	0.9421	−0.9845	−0.1605	−0.2029	
0.038 48	1.450	−1.224	−0.2298	−0.0042	0.0028
0.046 18	2.050	−1.449	−0.2825	0.3185	0.3230
0.053 87	2.738	−1.677	−0.3085	0.7524	0.7207
0.061 57	3.511	−1.913	−0.3228	1.276	1.269
0.069 26	4.365	−2.085	−0.3150	1.965	1.943
0.076 96	5.298	−2.214	−0.2847	2.799	2.745
0.115 44	11.07	−2.425	0.0244	8.668	8.516
0.153 92	18.54	−1.828	0.6805	17.39	17.20
0.230 88	38.06	1.632	3.149	42.84	43.42

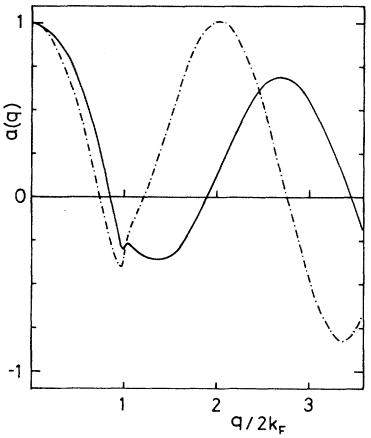

FIG. 1. Effective pseudopotential $a(q)=-[w(q)-v(q)v(q)]/[Z^*v(q)]$ in Be at $T=0$, for $\bar{n}/\bar{n}_0=1$ (solid curve) and 3 (dot-dashed curve).

cates that the present method is, on the 0-K isotherm, reasonably accurate and as reliable as the band-structure models.

C. Liquid metal

It has been shown elsewhere that the calculation of the excess entropy of a liquid metal is a good test of the quality of the pair interaction [4]. We have performed this calculation for Be. The parameters are the experimental values at the melting point under atmospheric pressure [29]:

$$T=1556\ \text{K},\quad \Omega=59.783\ \text{a.u.}\ .$$

The electronic density is $\bar{n}=0.033\,456$ a.u., and the compression $\Omega_0/\Omega=0.8714$. The experimental excess entropy is $S_{\text{exc}}/k_B=-3.55$. Ion-ion coupling is very strong at melting; the standard coupling parameter is $\Gamma=334$. The correct treatment of the bridge function is thus of great importance. We have solved the MHNC equations and found $S_{\text{exc}}/k_B=-3.07$. The non-negligible difference with respect to the experimental value reveals a situation analogous to that previously observed in sodium, with identical values of entropy, both theoretical and experimental. This may seem surprising for such different systems. It is nevertheless possible that the explanation is the same: a shift in the positions of the first node and first minimum of the interaction (of the order of 5% in Na). A uniform scaling $\phi(r)\rightarrow\phi(\lambda r)$, with $\lambda=0.95$ is enough to account for the experimental entropy of Na [4]. Unfortunately, there is no measurement of the structure factor $S(k)$ available for Be, so that we have no information about ϕ. The calculated $S(k)$ is shown in Fig. 2.

This incursion in the domain of liquid metals confirms a point already known: it is very difficult to construct a first-principles interaction which accurately reproduces the experiment. In this domain, only a qualitative agreement can be obtained.

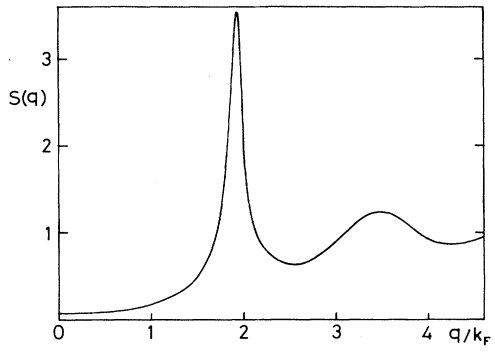

FIG. 2. Calculated ionic structure factor $S(q)$ for Be at melting under atmospheric pressure.

IV. DENSE BERYLLIUM PLASMA

The plasma EOS has been calculated on a grid of points defined by $\bar{n}/\bar{n}_0=0.2$-0.4-0.6-0.8-1.0-1.2-1.4-1.6-1.8-2.0-3.0-4.0-6.0 and $T(\text{eV})=2.5$-5-7.5-10-15-20-30-40-50-60-80-100. The change in the various contributions, their relative importance, can be appreciated on this grid, which allows us to illustrate the conditions of applicability of the model. We start with the results obtained for the ionization Z^*.

A. Ionization

Figure 3 shows the variations of Z^*. In the largest part of the domain, Be has only one bound level. So, at low temperature and normal density, Z^* is 2. But when the density increases enough, the $1s$ level delocalizes and a part of its charge density spreads outside the atomic

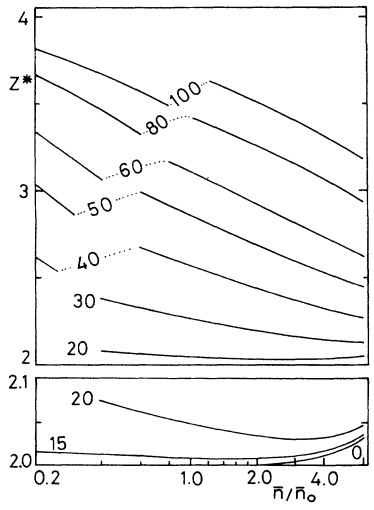

FIG. 3. Ionization Z^* in Be vs density for several temperatures. The numbers indicate temperatures in eV. The blank portions of curves correspond to regions where the model is not applicable.

TABLE III. Thermal electronic internal energy and pressure, in the present model (left column), and in the Thomas-Fermi model (right column). The ionization Z^* is also shown.

$\bar{n}/\bar{n}_0$	Z^*	$\beta\Delta E_s$		$\beta\Omega\Delta P_S$		Z^*	$\beta\Delta E_s$		$\beta\Omega\Delta P_S$	
			2.5 eV					7.5 eV		
0.4	2.0000	1.255	1.307	0.944	0.726	2.0000	1.955	2.596	1.308	1.309
0.8	2.0001	0.960	0.972	0.762	0.576	2.0001	1.727	2.171	1.212	1.203
1.2	2.0003	0.758	0.786	0.542	0.476	2.0004	1.559	1.907	1.079	1.105
2.0	2.0019	0.537	0.585	0.408	0.362	2.0020	1.314	1.560	0.927	0.943
4.0	2.0131	0.352	0.384	0.249	0.242	2.0132	0.959	1.106	0.665	0.692
6.0	2.0329	0.270	0.300	0.187	0.190	2.0330	0.774	0.880	0.531	0.558
			15 eV					30 eV		
0.4	2.0019	2.480	3.670	1.534	1.768	2.3818	4.684	5.035	2.000	2.353
0.8	2.0089	2.230	3.169	1.449	1.670	2.2939	3.983	4.414	1.871	2.227
1.2	2.0077	2.076	2.876	1.357	1.591	2.2481	3.609	4.067	1.778	2.147
2.0	2.0075	1.866	2.493	1.241	1.454	2.1962	3.166	3.635	1.657	2.026
4.0	2.0165	1.534	1.945	1.018	1.196	2.1405	2.593	3.037	1.454	1.804
6.0	2.0353	1.322	1.626	0.873	1.020	2.1243	2.269	2.675	1.319	1.636
			60 eV					100 eV		
0.4	3.0547	7.726	6.378	2.934	3.012	3.6729	8.216	6.972	3.520	3.426
0.8	3.1689	6.848	5.823	2.766	2.883	3.4929	7.617	6.482	3.362	3.301
1.2	3.0606	6.275	5.450	2.640	2.792	3.6316	7.279	6.223	3.276	3.232
2.0	2.9215	5.577	4.982	2.474	2.670	3.5099	6.741	5.823	3.125	3.122
4.0	2.7301	4.662	4.345	2.239	2.474	3.3127	5.943	5.247	2.900	2.946
6.0	2.6208	4.141	3.964	2.088	2.333	3.1819	5.451	4.893	2.752	2.825

TABLE IV. Comparison of the thermal electronic pressure $\beta\Omega\Delta P_S$ as obtained in the present model, in the INFERNO model [2,31], and in Thomas-Fermi theory (TF).

$\bar{n}/\bar{n}_0$	This work	INFERNO	TF	This work	INFERNO	TF
		2.5 eV			5 eV	
0.4	0.944	1.055	0.726	1.178	1.028	1.078
0.8	0.762	1.006	0.576	1.056	1.284	0.953
1.2	0.542	0.749	0.476	0.879	1.105	0.844
2.0	0.408	0.488	0.362	0.724	0.822	0.684
4.0	0.249	0.329	0.242	0.482	0.611	0.476
6.0	0.187	0.235	0.190	0.369	0.452	0.378
		10 eV			15 eV	
0.4	1.400	1.407	1.488	1.534	1.544	1.768
0.8	1.311	1.445	1.390	1.449	1.544	1.670
1.2	1.199	1.344	1.301	1.357	1.446	1.591
2.0	1.063	1.146	1.147	1.241	1.290	1.454
4.0	0.808	0.989	0.884	1.018	1.205	1.196
6.0	0.665	0.794	0.726	0.873	1.026	1.020
		20 eV				
0.4	1.644	1.649	1.992			
0.8	1.574	1.647	1.886			
1.2	1.487	1.547	1.809			
2.0	1.376	1.391	1.682			
4.0	1.174	1.350	1.438			
6.0	1.035	1.194	1.261			

sphere so that, according to Eq. (17), Z^* increases. The effect is not very pronounced in the range of densities studied here, but it was shown in Ref. [5] that the complete delocalization of the $1s$ state occurs around compression 50. When T increases, Z^* also increases at constant density. But for a given temperature, a higher density, starting from compression 0.2, causes first a decrease of Z^* because the $1s$ population increases (the quantity $\varepsilon_{1s}-\mu$ in the Fermi-Dirac statistical factor goes smaller). For a particular density, which is the limit of the degenerate domain for that temperature, μ becomes positive, $\varepsilon_{1s}-\mu$ starts to increase, and Z^* also increases. This behavior is typical of all the "average atom" models.

In Fig. 3 one can see a fast change in ionization for temperatures higher than 20 eV around a density going from $0.2\bar{n}_0$ (20 eV) to $\bar{n}_0$ (100 eV). This is a consequence of the new levels $2s$ and $2p$ appearing in the bound spectrum. As discussed in Sec. II C, the present model cannot follow entirely the transition of a level from a free to a bound state. The localization of the $n=2$ shell is anticipated by the formation of resonances in the free spectrum. Resonant states are expected to bring some contribution to the bound density. When they have crossed the zero-energy boundary, and as long as they are not well localized within the atomic sphere, they interact with neighboring bound states and may form molecular states that the model cannot take into account. The interactions involving more than two atoms may become important in such cases. For all these reasons, the model is thought to be inapplicable in the corresponding regions of the ρ-T plane. In the tabulations, blank rows will denote this situation.

B. Thermal electronic contribution

The free energy $F_S=F_0+F_1$ may be interpreted as that of a single atom, immersed in an electron gas, the ions being modeled by (i) the central ion in its cavity and (ii) a uniform background for the field ions. The last term F_{12} is the correction due to the more realistic description of the ionic distribution. Thus one can consider F_S as an electronic contribution comparable to that of other models using a simplified ionic distribution (isolated ion sphere, jellium with cavity, etc.). In Table III we compare the thermal part of the internal energy E_S and of the pressure P_S associated with F_S as obtained in the present model and in the Thomas-Fermi (TF) model. These thermal parts are

$$\beta\Delta E_S(\Omega,T)=\beta[E_S(\Omega,T)-E_S(\Omega,0)]\ , \tag{38a}$$

$$\beta\Omega\Delta P_S(\Omega,T)=\beta\Omega[P_S(\Omega,T)-P_S(\Omega,0)]\ , \tag{38b}$$

TABLE V. Comparison between the quantity $-[F_{\text{pair}}-\langle\phi\rangle]$, obtained in the present model (Be), Eqs. (23) and (24), and for a one-component Coulomb plasma (OCP) with same coupling Γ, using the analytical fit of Ref. [32]. Energies in Ry. $\bar{n}_0=0.038\,48$ a.u.

$\bar{n}/\bar{n}_0$	Γ	Be	OCP	Γ	Be	OCP	Γ	Be	OCP
		5 eV			10 eV			20 eV	
0.2	5.499	0.1916	1.316	2.750	0.2107	1.153			
0.4	6.928	0.3414	1.719	3.465	0.3282	1.525	1.841	0.3496	1.404
0.6	7.931	0.4694	2.007	3.966	0.4301	1.792	2.086	0.4272	1.641
0.8	8.729	0.5843	2.238	4.366	0.5224	2.008	2.282	0.4976	1.834
1.0	9.404	0.6874	2.435	4.703	0.6075	2.192	2.447	0.5627	1.999
1.2	9.995	0.7838	2.608	4.998	0.6867	2.354	2.592	0.6244	2.145
1.4	10.52	0.8741	2.764	5.263	0.7618	2.501	2.721	0.6828	2.276
1.6	11.01	0.9596	2.907	5.504	0.8328	2.635	2.839	0.7389	2.397
1.8	11.45	1.040	3.038	5.726	0.9006	2.759	2.948	0.7925	2.509
2.0	11.87	1.117	3.162	5.934	0.9657	2.876	3.049	0.8443	2.614
3.0	13.63	1.458	3.689	6.817	1.260	3.375	4.560	1.082	3.066
4.0	15.09	1.751	4.128	7.546	1.519	3.792	3.836	1.294	3.444
6.0	17.56	2.251	4.876	8.780	1.971	4.506	4.439	1.675	4.095
		40 eV			60 eV			100 eV	
0.2	1.077	0.5321	1.414	1.075	0.8272	2.115	0.806	1.022	2.412
0.4				1.170	0.9306	2.361	0.954	1.298	3.015
0.6	1.607	0.6843	2.364				1.037	1.403	3.362
0.8	1.705	0.7430	2.548	1.566	1.089	3.434	1.105	1.504	3.656
1.0	1.785	0.7964	2.701	1.635	1.148	3.626			
1.2	1.854	0.8463	2.833	1.692	1.199	3.787	1.350	1.694	4.736
1.4	1.915	0.8929	2.949	1.741	1.248	3.925	1.399	1.763	4.956
1.6	1.969	0.9372	3.054	1.784	1.292	4.047	1.441	1.825	5.148
1.8	2.018	0.9808	3.149	1.822	1.334	4.156	1.479	1.881	5.320
2.0	2.063	1.020	3.237	1.866	1.374	4.255	1.512	1.933	5.474
3.0	2.249	1.204	3.602	1.991	1.550	4.465	1.641	2.149	6.071
4.0	2.395	1.365	3.893	2.089	1.699	4.931	1.731	2.319	6.492
6.0	2.635	1.652	4.376	2.234	1.952	5.359	1.852	2.589	7.072

with $\Omega = Z^*(\bar{n},T)/\bar{n}$. At $T=0$, the electronic density is such that $\bar{n}' = Z(\bar{n}',0)/\Omega$. Both quantities are, at temperatures T and 0, calculated with the same volume, but different electronic densities. One can see that $\beta\Delta E_S$ of this model is smaller than its TF counterpart for T lower than 30 eV, and then larger for higher T. At 100 eV the two series of estimates are still not equivalent; the difference amounts to 18% for compression 0.4, and to 11% for compression 6. Up to 7.5 eV, the pressure is larger in this model, then weaker for higher T. The maximum difference reaches 20% around 30 eV, but at 100 eV the two series of results are very close. It appears from this brief comparison that the largest discrepancies between the two models affect the energy.

In Table IV we compare the thermal electronic component with that of the INFERNO model [2], computed by Pelissier [31]. Examination of the results does not reveal any general rule relating the differences between this model, INFERNO, and TF.

C. Ionic contribution

This component of the free energy requires the calculation of the pair interaction and the solution of the MHNC equations. In the domain studied here, the standard coupling parameter $\Gamma = (Z^*)^2/(k_B TR)$ varies in the range 1–35.

Table V reports values of $F_{\text{pair}} - \langle \phi \rangle$ [see Eqs. (23) and (24)] for all the densities of the grid and the temperatures 5, 10, 20, 40, 60, and 100 eV. They are compared with the same quantity for the OCP with the same coupling parameter Γ [32]. The differences are very important, due to strong electronic screening: the density parameter r_S goes from 3.14 to 1.01.

Figure 4 displays the free energy F_{12} versus $\bar{n}$ for several temperatures. The variations of this quantity have a much smaller amplitude than F_{pair}: at $T=2.5$ eV,

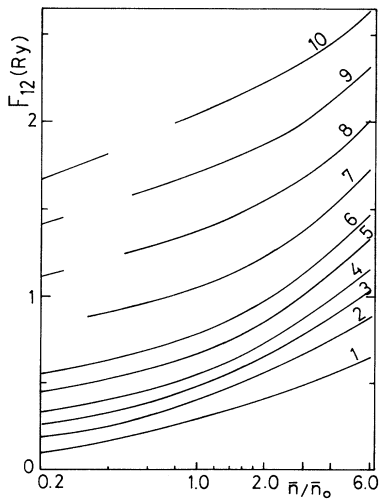

FIG. 4. Free energy F_{12}, Eq. (26), vs $\bar{n}/\bar{n}_0$ for various temperatures, in following order: 1, 2.5 eV; 2, 5 eV; 3, 7.5 eV; 4, 10 eV; 5, 15 eV; 6, 20 eV; 7, 30 eV; 8, 40 eV; 9, 50 eV; 10, 100 eV.

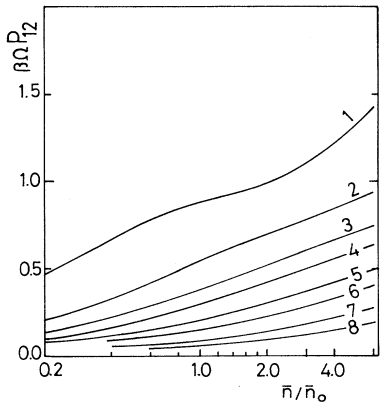

FIG. 5. Pressure $\beta\Omega P_{12}$ vs $\bar{n}/\bar{n}_0$ for several temperatures labeled as in Fig. 4.

for instance, F_{pair} varies between 0.022 and 1.78 Ry, while F_{12} varies between 0.088 and 0.644 Ry only. Similarly, at $\bar{n}=\bar{n}_0$, F_{pair} goes from 0.264 to 11.25 Ry for T between 2.5 and 100 eV, while F_{12} varies from 0.293 to 3.10 Ry only. This proves that F_{12} is a "good" quantity to deal with for computing numerical derivatives in order to get internal energy and pressure. Figure 5 shows the variations of P_{12}, the pressure associated with F_{12}. For the lowest temperatures, $\beta\Omega P_{12}$ reaches values of the order of 1, so that the total ionic contribution is twice the ideal contribution. It is not possible to detail here all the results, but we can say that, concerning the energy, βE_{12} can be as large as 2 at low temperature.

D. Complete EOS

Table VI gives results for the full EOS, including the ionic ideal contribution, for some densities and temperatures. In each case, comparison with a reference EOS is made. This reference EOS is made of the LMTO 0-K isotherm shown in Table I (with a rescaling on experiment around compression 1), together with the thermal TF electronic part and the ideal ionic part. The relative difference is

$$[E(\text{this work})/E(\text{reference}) - 1] \times 100$$

and there is a similar quantity for pressures. These relative differences reach 50% at $T=2.5$ eV, do not have a constant sign, and decrease when the temperature rises.

V. CONCLUSION

We have described an EOS model which attempts to treat the electronic and ionic terms in a coherent manner. This first-principles model makes use of well-known theories for the quantum-mechanical calculation of the electronic structure (DFT) and for the statistical mechanics of the ion subsystem (MHNC). Its validity is the same as that of the binary-force approximation between ions: it is warranted only if the electronic structure is "simple" and produces a metallic binding similar to that existing in

TABLE VI. Full equation of state for Be, Eqs. (33)–(36). For each temperature, the first column gives the compression, the second column gives βE in the present model, the third the difference with respect to the reference EOS defined in Sec. IV, in percent. The fourth and fifth columns are identical with the second and third columns, but for pressure $\beta\Omega P$. The compression is $c=\Omega_1/\Omega$, with $\Omega_1=52.0952$ a.u.

$\bar{n}/\bar{n}_0$	c	βE		$\beta\Omega P$	c	βE		$\beta\Omega P$	
			2.5 eV				7.5 eV		
0.4	0.401	1.787	19.0	1.744	51.0	0.401	3.197	−14.0	2.236	9.6
0.8	0.802	1.579	54.0	2.507	41.0	0.802	3.028	−2.1	2.515	14.0
1.2	1.203	1.755	59.0	3.413	28.0	1.203	3.055	5.6	2.821	14.0
2.0	2.003	2.682	45.0	5.364	19.0	2.003	3.322	14.0	3.447	15.0
4.0	3.983	6.442	24.0	10.57	12.0	3.983	4.452	19.0	5.035	13.0
6.0	5.917	10.78	17.0	15.58	9.2	5.916	5.799	18.0	6.597	11.0
			15 eV				30 eV		
0.4	0.399	3.890	−27.0	2.502	−4.9	0.337	6.088	−5.7	2.977	−10.0
0.8	0.798	3.669	−19.0	2.604	−1.8	0.699	5.343	−8.0	2.919	−9.6
1.2	1.198	3.623	−14.0	2.740	−0.4	1.070	5.013	−8.3	2.929	−9.2
2.0	1.997	3.697	−5.2	3.033	2.8	1.826	4.707	−7.6	3.004	−7.7
4.0	3.976	4.179	5.5	3.783	6.3	3.746	4.558	−4.2	3.292	−4.2
6.0	5.910	4.786	9.8	4.526	7.7	5.662	4.675	−1.0	3.618	−1.3
			60 eV				100 eV		
0.4	0.262	9.171	15.0	3.923	−1.3	0.218	9.837	14.0	4.565	3.5
0.8	0.506	8.282	12.0	3.780	−1.9	0.459	9.201	14.0	4.391	2.5
1.2	0.786	7.711	11.0	3.682	−2.8	0.662	8.846	13.0	4.322	2.3
2.0	1.372	7.037	8.7	3.591	−3.8	1.142	8.294	12.0	4.200	1.4
4.0	2.937	6.264	6.0	3.550	−4.2	2.421	7.534	10.0	4.061	0.3
6.0	4.589	5.923	4.7	3.599	−3.8	3.780	7.115	9.2	4.008	−0.1

a simple metal. Although some delocalization of the bound electronic levels can be accounted for by the model, complex effects such as molecular- or cluster-level formation, which involve charge redistribution and three (or more) ion interactions cannot be dealt with. The model reveals these effects through transitions of levels across the zero-energy boundary, and appearance of resonances in the free spectrum.

The model has been tested for Be on the 0-K isotherm where it gives good results, and at melting under normal pressure with a moderate degree of success similar to that of any first-principles theory in these conditions. It should be satisfactory in the plasma phase, when binary collisions are dominant. As with any theoretical EOS model, the global accuracy of the calculated thermodynamic functions is very difficult to assess. Only the use of the tabulations presented here in various numerical simulations of experiments will allow one to judge this accuracy.

It has been shown that there are several points in the density-temperature grid where the model is inapplicable. Examining the total energy and pressure curves does not allow one to detect any accident in the behavior of the thermodynamic functions around these points: the various components of E and P show irregularities but their sum is regular. Thus a normal interpolation should complete the tables without any particular difficulty. Finally, let us remark that, even for materials having a complex electronic structure in normal conditions, one can find domains in the ρ-T plane where this structure (with here the meaning of "NPA average electronic structure") becomes simple and lends itself to the use of the present model.

APPENDIX A: DETAILED EXPRESSION OF THE FREE ENERGY FOR EMBEDDING A NEUTRAL PSEUDOATOM IN THE FREE-ELECTRON GAS

The starting point is the expression of F_1 in Eq. (13). G is obtained from the kinetic internal energy and the entropy. The electron density is calculated by solving the effective one-particle equations for the potential V_t^*,

$$V_t^*=V^*+V_{\rm xc}(\bar{n}+\Delta n^*)-V_{\rm xc}(\bar{n}) .$$

The eigenvalues are ε_b (bound) and $\varepsilon=k^2/2$ (free). The occupation numbers are f_b (bound) and f_k (free). In the continuum the density of states is

$$\mathcal{N}(\varepsilon)=\mathcal{N}_0(\varepsilon)+\Delta\mathcal{N}(\varepsilon) , \tag{A1}$$

where $\mathcal{N}_0(\varepsilon)$ is the density of states of the uniform electron gas, and $\Delta\mathcal{N}(\varepsilon)$ its change due to the potential V_t^*, which can be written in terms of the phase shifts η_l of the eigenfunctions

$$\Delta\mathcal{N}(\varepsilon)d\varepsilon=\frac{2}{\pi}\sum_l(2l+1)\frac{d\eta_l}{dk}dk . \tag{A2}$$

The change in kinetic energy with respect to the uniform case is

$$\Delta T=\sum_b 2(2l_b+1)f_b\varepsilon_b+\int_0^\infty \Delta\mathcal{N}(\varepsilon)f_k\varepsilon\,d\varepsilon - (\bar{n}+\Delta n^*)\circ V_t^* \tag{A3}$$

and the change in entropy

$$\Delta S=-k_B\sum_b 2(2l_b+1)[f_b\ln f_b+(1-f_b)\ln(1-f_b)] -k_B\int_0^\infty \Delta\mathcal{N}(\varepsilon)d\varepsilon[f_k\ln f_k+(1-f_k)\ln(1-f_k)]\ . \tag{A4}$$

The change in the functional G is then obtained as

$$\Delta G=F_b+F_k-(\bar{n}+\Delta n^*)\circ V_t^*+F_{\rm xc}(\bar{n}+\Delta n^*)-F_{\rm xc}(\bar{n})\ ,$$

$$F_b=\sum_b 2(2l_b+1)[f_b\varepsilon_b+k_BTf_b\ln f_b +k_BT(1-f_b)\ln(1-f_b)]\ , \tag{A5}$$

$$F_k=\int_0^\infty \Delta\mathcal{N}(\varepsilon)d\varepsilon[f_k\varepsilon+k_BTf_k\ln f_k +k_BT(1-f_k)\ln(1-f_k)]\ .$$

Using the expression of the Fermi-Dirac occupation number with $\bar{\eta}=\beta\bar{\mu}[\bar{\mu}=\mu-V_{\rm xc}(\bar{n})]$, one arrives at

$$F_b=\bar{\mu}Z_b-k_BT\sum_b 2(2l_b+1)\ln[1+\exp(-\beta\varepsilon_b+\bar{\eta})]\ , \tag{A6}$$

$$F_k=\bar{\mu}Q_k-\frac{1}{\pi}\sum_l 2(2l+1)\int_0^\infty k\eta_l(k)f_k\,dk\ , \tag{A7}$$

with

$$Z_b=\sum_b 2(2l_b+1)f_b\ , \tag{A8}$$

$$Q_k=\frac{\beta}{\pi}\sum_l 2(2l+1)\int_0^\infty \eta_l(k)f_k(1-f_k)k\,dk\ . \tag{A9}$$

The total neutrality of the system imposes $Q_k=Z-Z^*-Z_b$ when the self-consistent solution is obtained. Z_b is the number of electrons in the bound part of the spectrum. Then the electrostatic terms contained in F_1 have to be evaluated together with the term $-(\bar{n}+\Delta n^*)\circ V_t^*$ in G. They are reexpressed

$$W=-\tfrac{1}{2}(2\bar{n}+\Delta n^*)\circ U-\tfrac{1}{2}\Delta Z\left[\frac{1}{r}\circ\Delta n^*\right]-3\Delta ZZ^*/2R -3(Z^*)^2/5R+\Delta ZV_{\rm xc}(\bar{n})+M_{\rm xc}\ , \tag{A10}$$

with

$$\Delta Z=Z-Z^*\ , \tag{A11}$$

$$U=-\frac{\Delta Z}{r}+\frac{1}{r}*\Delta n^*\ , \tag{A12}$$

$$V_{\rm xc}(n)=dF_{\rm xc}(n)/dn\ , \tag{A13}$$

$$M_{\rm xc}=(n+\Delta n^*)\circ V_{\rm xc}(\bar{n}+\Delta n^*)-\bar{n}\circ V_{\rm xc}(\bar{n})\ . \tag{A14}$$

Finally, one gets for the embedding free energy

$$F_1=F_b+F_k+W+F_{\rm xc}(\bar{n}+\Delta n^*)-F_{\rm xc}(\bar{n}) \tag{A15}$$

and for the internal energy

$$\tilde{E}_1=E_b+E_k+W+E_{\rm xc}(\bar{n}+\Delta n^*)-E_{\rm xc}(\bar{n})\ , \tag{A16}$$

$$E_b=\sum_b 2(2l_b+1)f_b\varepsilon_b\ , \tag{A17}$$

$$E_k=-\frac{1}{\pi}\sum_l 2(2l+1)\int_0^\infty \eta_l(k)[1-\beta\varepsilon(1-f_k)]f_k k\,dk\ . \tag{A18}$$

APPENDIX B: EXPRESSION OF THE TOTAL FREE ENERGY (FOR A GIVEN SET OF IONIC POSITIONS)

This expression is established by summing the contributions in Eqs. (14a)–(14c), using the expansion of Eq. (15),

$$F_e=G[\bar{n}]+\sum_i G_i+\tfrac{1}{2}\sum_{ij}{}'(Z^2/R_{ij}+G_{ij}) +\left[\bar{n}+\sum_i\Delta n_i^*\right]\circ\frac{1}{r}*\left[\sum_j -Z\delta_j\right] +\frac{1}{2}\left[\bar{n}+\sum_i\Delta n_i^*\right]\circ\frac{1}{r}*\left[\bar{n}+\sum_j\Delta n_j^*\right] -\frac{1}{2}\left[\bar{n}-\sum_i m_i\right]\circ\frac{1}{r}*\left[\bar{n}-\sum_j\nu_j\right]\ . \tag{B1}$$

Isolating the diagonal terms $i=j$ in this expression, using Eq. (13) for F_1, it is easy to show that

$$F_e=G[\bar{n}]+\sum_i F_1+\tfrac{1}{2}\sum_{ij}{}'\phi_{ij}+\tfrac{1}{2}\sum_i(\nu_i-\bar{n})\circ\frac{1}{r}*(\nu_i-m_i) +\sum_i(\bar{n}-\nu_i)\circ V_i^*\ , \tag{B2}$$

where V_i^* is defined in Eq. (4b); ϕ_{ij} is a binary interaction

$$\phi_{ij}=G_{ij}+(-Z\delta_i+\Delta n_i^*)\circ\frac{1}{r}*(-Z\delta_j+\Delta n_j^*) -\nu_i\circ\frac{1}{r}*m_j\ . \tag{B3}$$

One can see that all the one-center terms are equal, so that

$$F_e/N=F_0+F_1+\tfrac{1}{2}\sum_j{}'\phi(R_j)+(\bar{n}-\nu)\circ V^* -\tfrac{1}{2}(\bar{n}-\nu)\circ\frac{1}{r}*(\nu-m)\ , \tag{B4}$$

with, as in Eqs. (13) and (16b),

$$F_0=Z^*g(\bar{n},T)\ , \tag{B5}$$

$$F_1=G[\bar{n}+\Delta n^*]-G[\bar{n}]+\left[-\frac{Z}{r}\right]\circ(\Delta n^*+\nu) +\tfrac{1}{2}(\Delta n^*+\nu)\circ\frac{1}{r}*(\Delta n^*+\nu)\ . \tag{B6}$$

The quantity $\sum_j'\phi(R_j)$ is the only one depending on the ionic structure.

[1] G. I. Kerley, Sandia National Laboratories Report No. SAND88-2291, 1991 (unpublished).
[2] D. A. Liberman, Phys. Rev. B **20**, 4981 (1979).
[3] L. Dagens, J. Phys. (Paris) **34**, 879 (1973).
[4] F. Perrot and G. Chabrier, Phys. Rev. A **43**, 2879 (1991).
[5] F. Perrot, Phys. Rev. A **42**, 4871 (1990).
[6] P. Hohenberg and W. Kohn, Phys. Rev. **136**, B864 (1964); W. Kohn and L. J. Sham, *ibid.* **140**, A1133 (1965); N. D. Mermin, *ibid.* **137**, A1441 (1965).
[7] H. Iyetomi and S. Ichimaru, Phys. Rev. A **34**, 433 (1986).
[8] J. Friedel, Philos. Mag. **43**, 153 (1952); Adv. Phys. **3**, 446 (1954); L. Dagens, J. Phys. C **5**, 2333 (1972); F. Perrot, Phys. Rev. A **25**, 489 (1982); **26**, 1035 (1982).
[9] M. W. C. Dharma-wardana and F. Perrot, Phys. Rev. A **45**, 5883 (1992).
[10] N. W. Ashcroft and D. Stroud, in *Solid State Physics: Advances in Research and Applications,* edited by H. Ehrenreich, F. Seitz, and D. Turnbull (Academic, New York, 1978), Vol. 33, p. 1.
[11] S. Ichimaru, H. Iyetomi, and S. Tanaka, Phys. Rep. **149**, 91 (1987); X. Z. Yan, S. Tsai, and S. Ichimaru, Phys. Rev. A **43**, 3057 (1991).
[12] M. W. C. Dharma-wardana and F. Perrot, Phys. Rev. A **26**, 2096 (1982).
[13] J. Chihara, Phys. Rev. A **33**, 2575 (1986).
[14] H. E. DeWitt and F. J. Rogers, Phys. Lett. A **132**, 273 (1988).
[15] D. Ofer, E. Nardi, and Y. Rosenfeld, Phys. Rev. A **38**, 5801 (1988).
[16] Y. Rosenfeld and N. W. Ashcroft, Phys. Rev. A **20**, 1208 (1979).
[17] F. Lado, S. M. Foiles, and N. W. Ashcroft, Phys. Rev. A **28**, 2374 (1983).
[18] L. Verlet and J. J. Weis, Phys. Rev. A **5**, 939 (1972).
[19] D. Henderson and E. W. Grundke, J. Chem. Phys. **63**, 601 (1975).
[20] M. W. C. Dharma-wardana and G. C. Aers, Phys. Rev. B **28**, 1701 (1983).
[21] M. W. C. Dharma-wardana, G. C. Aers, P. W. M. Jacobs, Z. A. Rycerz, and K. E. Larson, Phys. Rev. A **37**, 4500 (1988).
[22] J. Chihara, Phys. Rev. A **40**, 4507 (1989).
[23] M. Dzugutov, Phys. Rev. A **40**, 5434 (1989).
[24] M. W. C. Dharma-wardana and F. Perrot, Phys. Rev. Lett. **65**, 76 (1990).
[25] F. Perrot, Phys. Rev. A **44**, 8834 (1991).
[26] L. C. Ming and M. H. Manghnani, J. Phys. F **14**, L1 (1984).
[27] J. Meyer-ter-Vehn and W. Zittel, Phys. Rev. B **37**, 8674 (1988).
[28] F. Perrot, Phys. Rev. B **21**, 3167 (1980).
[29] D. R. Stull and G. C. Sinke, *Thermodynamic Properties of the Elements,* Advances in Chemistry Series Vol. 18 (American Chemical Society, Washington, D.C., 1956).
[30] V. L. Moruzzi, J. F. Janak, and A. R. Williams, *Calculated Properties of Metals* (Pergamon, New York, 1978).
[31] J. L. Pelissier (private communication).
[32] W. L. Slattery, G. D. Doolen, and H. E. DeWitt, Phys. Rev. A **21**, 2087 (1980); G. S. Stringfellow, H. E. DeWitt, and W. L. Slattery, Phys. Rev. A **41**, 1105 (1990).